УДК 551.461

© *Е. А. Рувинская*[1], *О. Е. Куркина*[1], *А. А. Куркин*[1], *А. И. Зайцев*[1,2]
[1]Нижегородский государственный технический университет им. Р. Е. Алексеева
[2]Специальное конструкторское бюро средств автоматизации морских исследований ДВО РАН, г. Южно-Сахалинск
aakurkin@gmail.com

МОДЕЛИРОВАНИЕ ВОЗДЕЙСТВИЯ ВНУТРЕННИХ ВОЛН НА МОРСКИЕ ПЛАТФОРМЫ ДЛЯ ГИДРОЛОГИЧЕСКИХ УСЛОВИЙ ШЕЛЬФОВОЙ ЗОНЫ о. САХАЛИН

Статья поступила в редакцию 04.11.2017, после доработки 09.11.2017.

Оцениваются динамические нагрузки на подводные вертикальные цилиндрические части морских платформ при воздействии полнонелинейных внутренних волн, генерируемых многокомпонентным баротропным приливом, распространяющимся вдоль вертикального разреза над неровностями дна в условиях Охотского моря (залив Анива, юго-восточная часть шельфовой зоны острова Сахалин). Эволюция этого процесса анализируется с помощью численной модели для уравнений Эйлера, описывающих движение несжимаемой стратифицированной по плотности жидкости в вертикальной плоскости. Интенсивность силы давления на подводную боковую поверхность опоры морской платформы и ее расчетный изгибающий момент выражаются в соответствии с формулой Морисона для цилиндрической сваи диаметром 2.5 м и высотой 42 м и рассчитаны как функции времени. Во время приливного цикла эти характеристики могут достигать значений $2.3 \cdot 10^5$ Н и $4.8 \cdot 10^6$ Н·м, соответственно. Определена также частота появления больших пиковых значений в поле скорости внутренних волн и вероятности соответствующих этим пикам высоких нагрузок. Значительная неравномерность распределения скорости, а также динамических нагрузок по глубине является типичной особенностью воздействия внутренних волн.

Ключевые слова: внутренние волны, сила сопротивления, сила инерции, крутящий момент, уравнение Морисона, придонная скорость.

E. Rouvinskaya[1], *O. Kurkina*[1], *A. Kurkin*[1], *A. Zaytsev*[1,2]
[1]Nizhny Novgorod State Technical University n. a. R. E. Alekseev, Nizhny Novgorod, Russia
[2]Special Research Bureau for Automation of Marine Researches, Far Eastern Branch of Russian Academy of Sciences, Yuzhno-Sakhalinsk, Russia

MODELING OF INTERNAL WAVE ACTION ON OFFSHORE PLATFORMS FOR HYDROLOGICAL CONDITIONS OF THE SAKHALIN SHELF ZONE

Received 04.11.2017, in final form 09.11.2017.

Dynamical loads are estimated on underwater vertical cylindrical parts of offshore platforms from the forcing of fully nonlinear internal wave motions generated by multicomponent barotropic tidal flow over topography along a vertical section for the conditions of the Sea of Okhotsk (Aniva Bay, near the south-eastern part of the Sakhalin Island shelf). The evolution of this process is analysed using numerical model of Euler equations for incompressible density-stratified fluid in a vertical plane. The intensity of pressure on lateral underwater surface and the rate inertia moment are expressed according to Morison's formula for a cylindrical pile of 2.5 m diameter and 42 m height and computed as functions of time. They can reach values of $2.3 \cdot 10^5$ N and $4.8 \cdot 10^6$ N·m, respectively, during the tidal cycle. The frequency of the appearance of large peak values in the internal wave velocity field and the probabilities of the corresponding high loads are also calculated.

Key words: internal waves, drag force, inertial force, torque, Morison equation, near-bottom velocity.

Ссылка для цитирования: *Рувинская Е. А., Куркина О. Е., Куркин А. А., Зайцев А. И.* Моделирование воздействия внутренних волн на морские платформы для гидрологических условий шельфовой зоны о. Сахалин // Фундаментальная и прикладная гидрофизика. 2017. Т. 10, № 4. С. 61—70.

For citation: *Rouvinskaya E., Kurkina O., Kurkin A., Zaytsev A.* Modeling of internal wave action on offshore platforms for hydrological conditions of the Sakhalin shelf zone. *Fundamentalnaya i Prikladnaya Gidrofizika.* 2017, 10, 4, 61—70.

DOI: 10.7868/S2073667317040062.

Internal gravity waves play an important role in the dynamics of water masses and ecosystems: they have a significant influence on mixing of water layers, suspending and moving sedimentary materials [1—2], significantly determine nutrient distribution and biological productivity [3—5]. Sea water density field distortions caused by internal waves affect the propagation of acoustic signals over long distances anomalously amplifying sound losses for particular frequencies [6, 7]. The currents induced by internal waves on continental shelfs seriously affect the underwater parts of offshore platforms, strengthening tension of anchoring nodes [8, 9], that call into question the safety of these engineering constructions [10, 11]. The velocities induced by internal waves can produce significant local concentrated loads, bending and twisting moments [12—17] on the cantilever beams supporting a drilling rig and oil platforms. There are cases when, under the influence of internal waves, the oil platforms are displaced 200 m in the horizontal and 10 m in the vertical direction. Nonlinear internal waves can cause a significant increase (up to twice) in the tension of the anchor chains [14] used in spar platforms. The intensity of influence of such a wave with a maximum horizontal velocity of 2.1 m/s is comparable with the influence of a surface wave with a length of about 300 m and a height of 18 m [18]. The results of field observations in the South China Sea suggest that intensive internal waves induce significantly greater loads and torques in offshore platform than surface waves. The danger of such waves is recognized as critical, so development and adaptation of models which allow estimating a risk of the intense internal wave's impact on the offshore platforms is an actual and practically significant task.

When underwater structures are flowed around by a current induced by internal gravity waves, the intensity of the side surface pressure on offshore platform is usually calculated approximately according to the Morison equation [9, 19—23]. In the framework of this approach flow pressure contains the inertial (linear, depending on the acceleration of fluid particles in the wave) and the velocity (non-linear resistance force, quadratic in velocity) components. This method firstly was suggested in [24] to evaluate the forces associated with surface waves and influencing on vertical cylindrical objects in water, supports, piles or pillars, supposing that the cylinder diameter, D, is much smaller than the typical wavelength L so that the wave field almost doesn't "feel" the pillar. Let us consider in more details the application of this method to estimate the impact of internal waves on the offshore platforms.

Mathematical model of internal wave impact on pillars. Following [25], we consider small oscillations in the vertical plane (x, z) of a cylinder submerged into water (fig. 1).

It is assumed that the distribution of masses inside the cylinder can be generally inhomogeneous. The equations of motion of the cylinder are:

$$m\frac{d^2x_c}{dt^2} = X\,,\ m\frac{d^2z_c}{dt^2} = Z\,,\ J\frac{d^2\varphi}{dt^2} = M\,, \tag{1}$$

where m is mass of the cylinder, J is the moment of inertia with respect to cylinder's center of gravity, x_c, z_c, φ are coordinates of the center of gravity and the rotation angle of the cylinder centerline, X, Z are the projections of the external forces and M is their moment relative to the center of gravity. When we calculate the values of X, Z, M in (1), associated with the water pressure under the influence of flow around the cylinder, we assume that the pressure is exerted only by the normal component of the flow, v_n, w_n. The intensity $f_n(s)$ of pressure on the lateral surface of cylinder is calculated by the well-known Morison formula [19—21] and contains inertial f_I and velocity f_D components

$$f_n(s,t) = f_I + f_D\,,\ f_I(t) = \rho g S C_M a_n\,,\ f_D(t) = \rho g R C_D\,|\,\nu_n^e\,|\,\nu_n^e\,, \tag{2}$$

where s is coordinate along the cylinder axis, s = 0 corresponds to the center of mass of the cylinder (fig. 1),

$$\nu_n^e = \nu_n - \nu_n^c\,,\ \nu_n = u(s,t)\cos\varphi + w(s,t)\sin\varphi\,,\ a_n = \frac{d\nu_n}{dt}\,,\ v_n^c = \frac{dx_c}{dt}\cos\varphi + \frac{dz_c}{dt}\sin\varphi + s\frac{d\varphi}{dt}\,.$$

Here v^e_n is relative normal projection of the velocity at point s on the cylinder centerline, v_n and an are projections of the velocity and acceleration of water, $u(s, t)$ and $w(s, t)$ calculated at the point $x = x_c + s\sin\varphi$, $z = z_c + s\cos\varphi$, v^c_n is projection of the velocity of the cylinder centerline's point s, $S = \pi R^2$ is cross-sectional area, R is radius of the cylinder, constants C_D and C_M are empirical, averaged over the typical period of the wave drag and inertia coefficients, respectively. They can be defined for a wide range of control parameters: the Kelegan—Carpenter number K ($= U_mT/D$), the Reynolds number Re ($= U_mD/\nu$) and the relative roughness

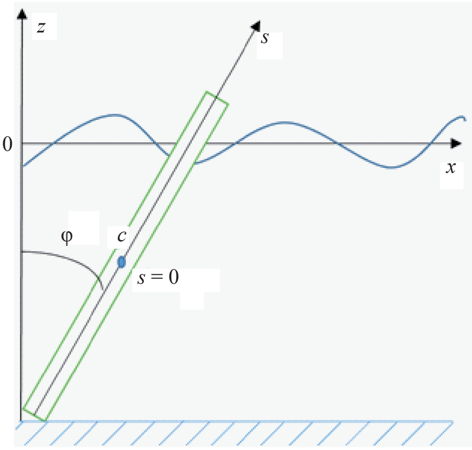

Fig. 1. A cylinder submerged into water.

Рис. 1. Погруженный в воду цилиндр.

k/D, where D is the diameter of the circular cylinder, U_m is maximum flow velocity, T is the typical period of oscillations in the flow, ν is the kinematic viscosity, k is the average size of the irregularities.

The force F_n directed by the normal to the cylinder axis and the moment M' are obtained by integrating over the length of the underwater part of the cylinder

$$F_n(t) = \int_{s_1}^{s_0} f_n(s)ds\,,\; M'(t) = \int_{s_1}^{s_0} f_n(s)s\,ds\,, \tag{3}$$

where $s_1 < 0$ corresponds to the lower end of the cylinder, and $s_0 > 0$ is the point of intersection the cylinder axis and the sea surface. If the cylinder is assumed to be stiff (the bending angles are small) and is fixed at the bottom, then $s \equiv z$, and the integration in (3) can be carried out over the entire water column in case when the cylinder is longer than the sea depth, and over the entire height of the cylinder when it is completely submerged.

The force F_n and the moment M' can be easily determined if the velocity, normal to the cylinder, and acceleration components are known. In the case of small oscillations, this is the horizontal velocity component u and its time derivative — an acceleration $a_n = \partial u/\partial t$, which can be easily calculated.

To compute the integrals (3), the normal velocity and acceleration must be known for the whole range of values of the vertical coordinate z, which is not always possible for experimental data and field observations, or the resolution can be inadequate. Therefore, preliminary theoretical estimates play here a very important role. Integration can be done using the Simpson method, with the help of standard utilities.

It should be noted that the representation of the flow pressure force on the cylinder (2) at the point in the form of a sum of two components f_I and f_D is valid only approximately. Such a separation is semi-empirical and requires in each case an experimental proof. It is not uniform in all possible ranges of K, Re and k/D. More general formulations for forces acting on a solid submerged in a fluid body were presented by Lighthill [26] in terms of both velocity and vorticity. It was shown that the viscous drag force and the inviscid inertia force are not independent, and that the appearance and diffusion of vorticity influences on both components of the force in a nonstationary flow. In this case, even the coefficient of inertia (or the coefficient of the added mass), C_M, is not constant and varies in time, even during the oscillation period of the flow, and also when the control parameters (Re, K, k/D, shape and orientation of the body) are changing. However, this simplified approach is useful for the first rough estimates of dynamical loads from wave-induced currents on underwater engineering structures.

Numerical modelling of internal gravity wave dynamics on the Sakhalin shelf. The main goal of this work is to study the influence of internal gravity waves on the pillars of offshore platform. The following tasks are solved for this purpose:

— initialization of the background conditions in the numerical model: temperature, salinity, pressure, water level fluctuations, bathymetry data were processed (data records were made by Sakhalin Research Institute of Fisheries and Oceanography, Russia in the summer in the southern part of the Sakhalin continental slope in 1999—2003 years (the data were kindly provided by Dr. A. G. Chernov through personal communications);

— modeling internal wave dynamics in oceanographic conditions that correspond to the shelf zone of Sakhalin Island in the Sea of Okhotsk;

— estimation of internal waves' impact on pillars of offshore platforms on the basis of the predicted velocity fields induced by internal waves.

Study of internal waves' dynamics was carried out in the framework of program code intended for numerical modeling of propagation and transformation of such waves in the ocean, that implements procedure of numerical integration of fully nonlinear two-dimensional (vertical plane) system of equations of hydrodynamics inviscid incompressible stratified fluid in the Boussinesq approximation bearing in mind the impact of barotropic tide [27]:

$$\vec{V}_t + (\vec{V}\nabla)\vec{V} - f\vec{V} \times \vec{k} = -\nabla P - \vec{k}\rho g \,, \tag{4}$$

$$\rho_t + \vec{V}\nabla\rho = 0 \,, \tag{5}$$

$$\nabla\vec{V} = 0 \,, \tag{6}$$

$$\rho = \frac{\rho_f - \rho_0}{\rho_0} \,, \tag{7}$$

where $\vec{V}$ (u, v, w) is the velocity vector, ∇ is the three dimensional vector gradient operator, subscript t denotes the time derivative, ρ_f is the density of sea water, ρ_0 is the average or characteristic density (introduced owing to the Boussinesq approximation that assumes that the density $\rho_f = \rho_0(1 + \rho)$ only changes insignificantly in the basin and ρ is a nondimensional quantity that has a meaning of density anomaly), P is the pressure, g is acceleration due to gravity, f is, as above, the Coriolis parameter and $\vec{k}$ is the unit vector along the z-direction. The waves propagate in the x-direction, y-axis is perpendicular to the wave motion and z is the depth.

The normal to the wave propagation (cross-section) velocity is included in the model, but no variation along the y-coordinate is allowed. This is realised by neglecting the partial derivatives with respect to y in the basically three-dimensional equations (4)—(7). The equations are transformed to a terrain-following coordinate system (so-called sigma-coordinates). The equations are solved over a covered by a rigid lid at the surface.

To initialize the model, it is necessary to prescribe horizontally homogeneous density field of water masses $\rho_{mean}(z)$ as well as the velocity distribution in the barotropic tidal field in the computational domain. The steps of the numerical scheme in space and time are chosen to satisfy the Courant—Friedrich—Levy criterion for stability.

To determine water depth, we used high resolution bathymetry data between 140 and 150 degrees west longitude and 40 and 50 degrees north latitude, which were provided by SakhNIIRO. Then we defined a section between the points 142.65E, 46.5N and 143.05E, 46.05N in the shelf of Sakhalin Island area (Aniva Bay). Its length is 58 km. The direction of the section is determined in accordance with the pattern of internal gravity wave refraction from the tidal front, obtained with a linear ray model. Since horizontally-homogeneous density field is used in our numerical model, the density profile from the outer edge of the section was taken, which is obtained by approximating and averaging of in-situ data on temperature, salinity and pressure from the sensors. Detailed description of algorithm of this stage is presented in [28]. Density anomaly field, bathymetry for chosen section and position of a pile are shown in fig. 2.

An important condition for initialization of the model is the structure of the barotropic tide. The horizontal velocity ubtr in the barotropic tide is given by:

$$u_{btr} = \frac{H}{r(x)}\sum_i U_{\max_i} \sin(\sigma_i t + \psi_i) = \sum_i \frac{Q_i}{r(x)} \sin(\sigma_i t + \psi_i), \tag{8}$$

$$Q_i = U_{\max i} H \,, \tag{9}$$

$$U_{\max i} = \sqrt{\frac{g}{H}}\eta_i \,, \tag{10}$$

here Q_i is the maximum cross flux of water for the corresponding component of the tide, $r(x) = H - h(x)$ is the local depth of the fluid, $h(x)$ is bathymetry, H is vertical size of the physical domain, σ_i is the frequency

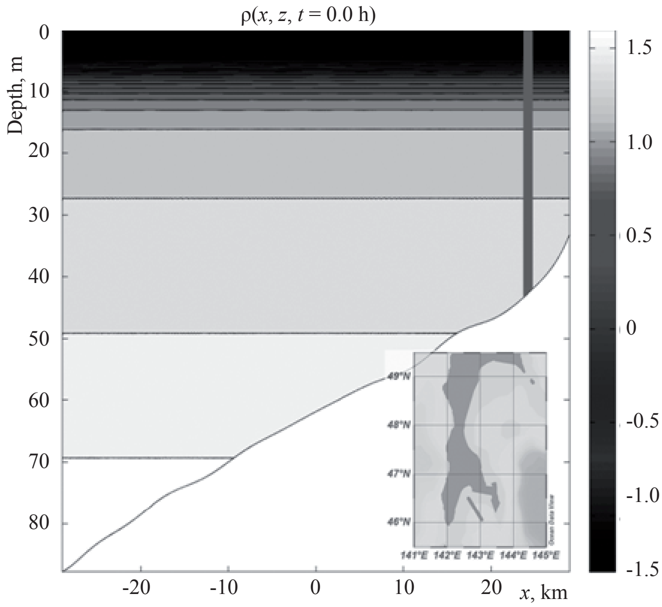

Fig. 2. Density anomaly field, bathymetry and position of hypothetic pile.

Рис. 2. Поле аномалии плотности, батиметрия и расположение гипотетической опоры.

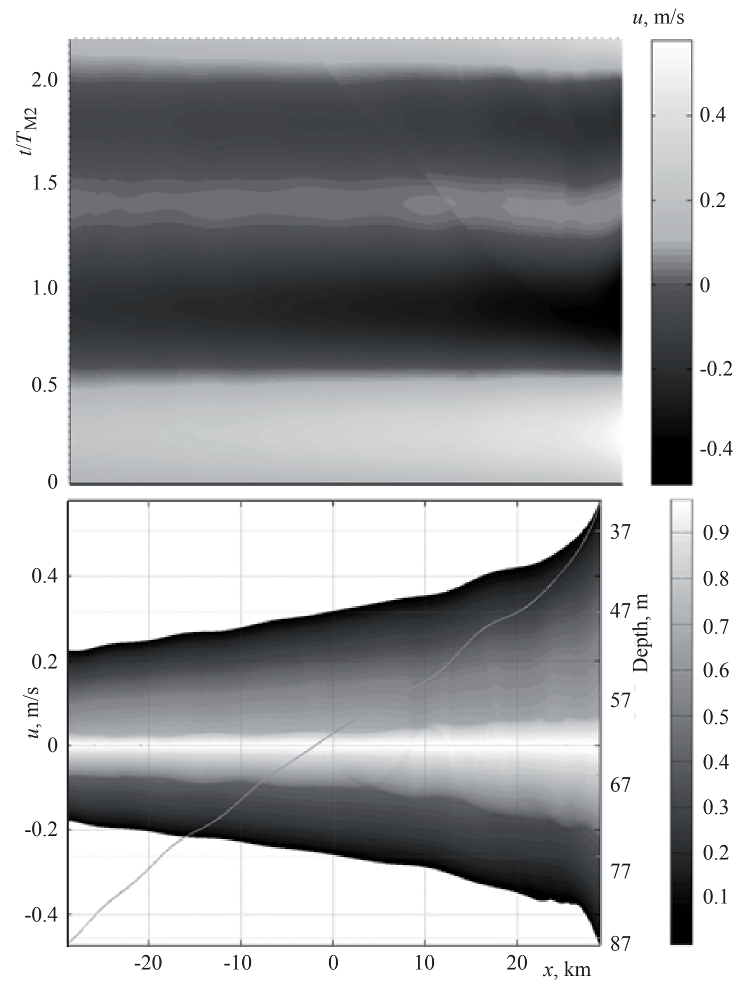

Fig. 3. x-t diagram of the total velocity in the projection on the tangent to the bottom line (upper panel) and the exceedance probability distribution for absolute values of horizontal velocity (lower panel; gray line — bottom relief).

Рис. 3. Пространственно-временная диаграмма полной скорости в проекции на касательную к линии дна (вверху) и распределение вероятности превышения уровня для абсолютных значений горизонтальных скоростей (внизу; серая линия — рельеф дна).

of the tidal component, ψ is its initial phase, and the *i*-index indicates the various tidal components (M2, N2, etc.). The flow velocities of the components in the barotropic tide are calculated from the data on the tidal level rise η_i. From the continuity equation we obtain the expression for the vertical velocity of the barotropic tide

$$w_{btr} = \sum_i Q_i \frac{dr}{dx} \frac{(z-H)}{r^2(x)} \sin(\sigma_i t + \psi_i). \tag{11}$$

The barotropic tide velocity $v_{\rm btr}$ in the transverse direction with respect to our section is given by:

$$v_{btr} = \sum_i \frac{f Q_i}{\sigma_i r(x)} \cos(\sigma_i t + \psi_i). \tag{12}$$

In accordance with (8)—(12), the initial velocity field is initialized as follows (there are no internal waves at the initial time):

$$u = \sum_i \frac{Q_i}{r(x)} \sin(\psi_i),\; v = \sum_i \frac{f Q_i}{\sigma_i r(x)} \cos(\psi_i),\; w = \sum_i Q_i \frac{dr}{dx} \frac{(z-H)}{r^2(x)} \sin(\psi_i).$$

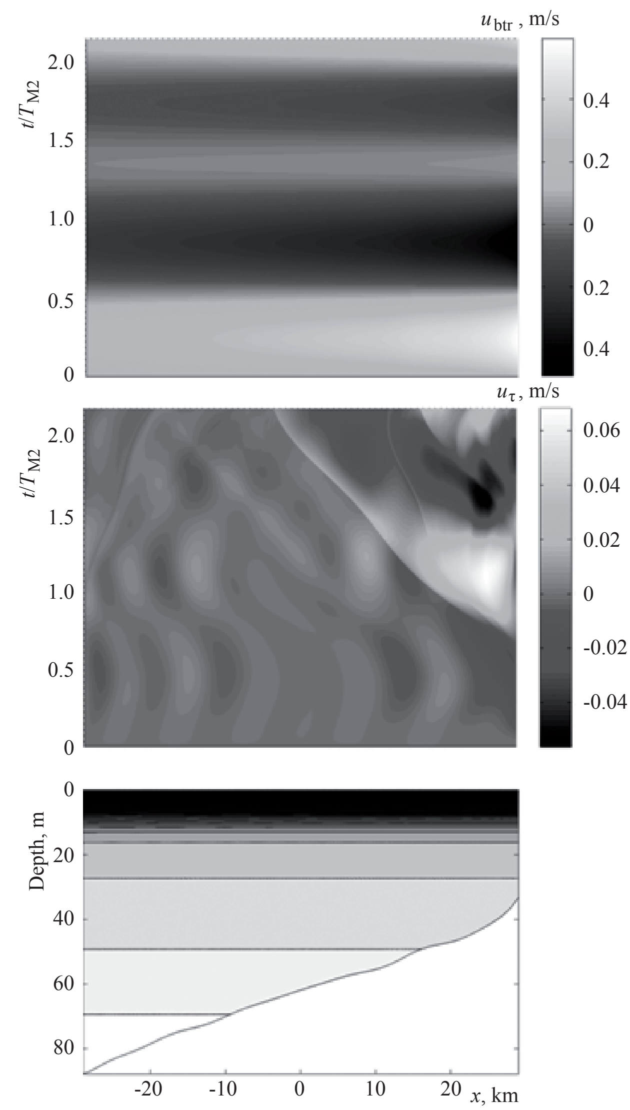

Fig. 4. x-t diagram of the velocity of the barotropic tide (upper panel) and horizontal baroclinic velocity component (middle panel) for chosen section.

Рис. 4. Пространственно-временная диаграмма скорости баротропного прилива (вверху) и горизонтальной бароклинной компоненты скорости (в середине) для выбранного разреза.

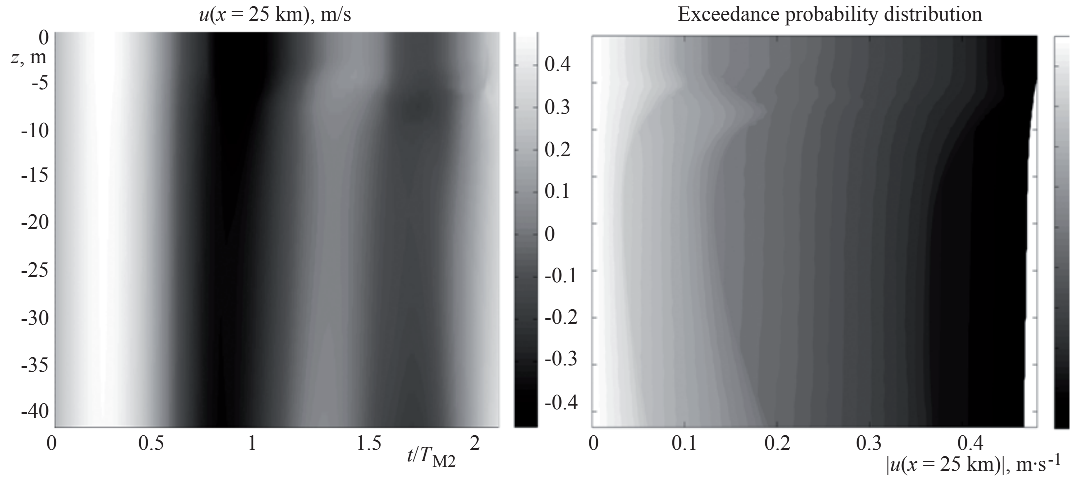

Fig. 5. The total velocity at the location of hypothetic pile throughout the vertical depending on time (at the left) and exceedance probability distribution for absolute values of horizontal velocity at the location of hypothetic pile over the fluid column (on the right).

Рис. 5. Полная скорость в месте расположения гипотетической опоры по глубине в зависимости от времени (слева) и распределения вероятности превышения уровня для абсолютных значений горизонтальной скорости в месте расположения гипотетической сваи (справа).

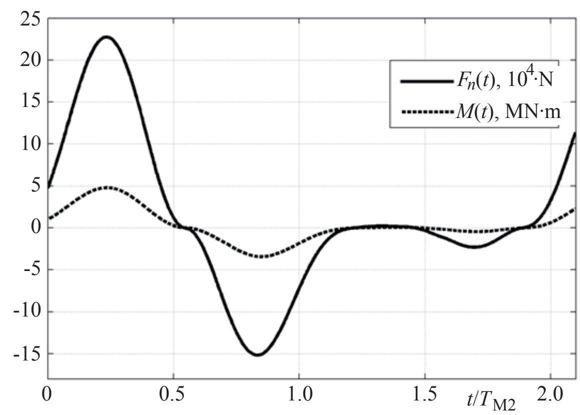

Fig. 6. The total force and the moment of force with respect to a bottom at the location of hypothetic pile depending on time.

Рис. 6. Полная сила и момент силы относительно дна в месте расположения гипотетической опоры в зависимости от времени.

The barotropic tide was initialized as a superposition of the components M2, N2, Q1, O1, P1, K1 [29]. The Coriolis parameter for the considered sea area is $f = 0.0001051$ s^{-1}.

For engineering applications, it is of great interest to estimate the contribution of internal waves to the formation of near-bottom currents, so we have analyzed the structure of the tangential to the bottom velocities for this model case. We defined the projection of the total velocity on the tangent to the bottom and obtained its time dependence at each point of the cross-section (fig. 3). The distribution of positive and negative values of the total velocity is essentially asymmetric, especially to the right of the point $x = 20$ km. This indicates the nonlinearity of the process. The x-t diagrams for the velocities of the near-bottom barotropic tidal flow and the baroclinic horizontal velocity component of the wave field are shown in fig. 4. The contribution of the wave component into the total horizontal velocity is rather small for our model case. The maximum values of the bottom current velocities in the field of internal waves near the right bound are nearly ten times smaller than the velocities of the barotropic tidal current for the considered situation. But the internal wave component of the near-bottom velocity has a more complex, irregular spatio-temporal structure. However, structure of the current in the shallower part of the section is again determined mainly by the barotropic tidal flow.

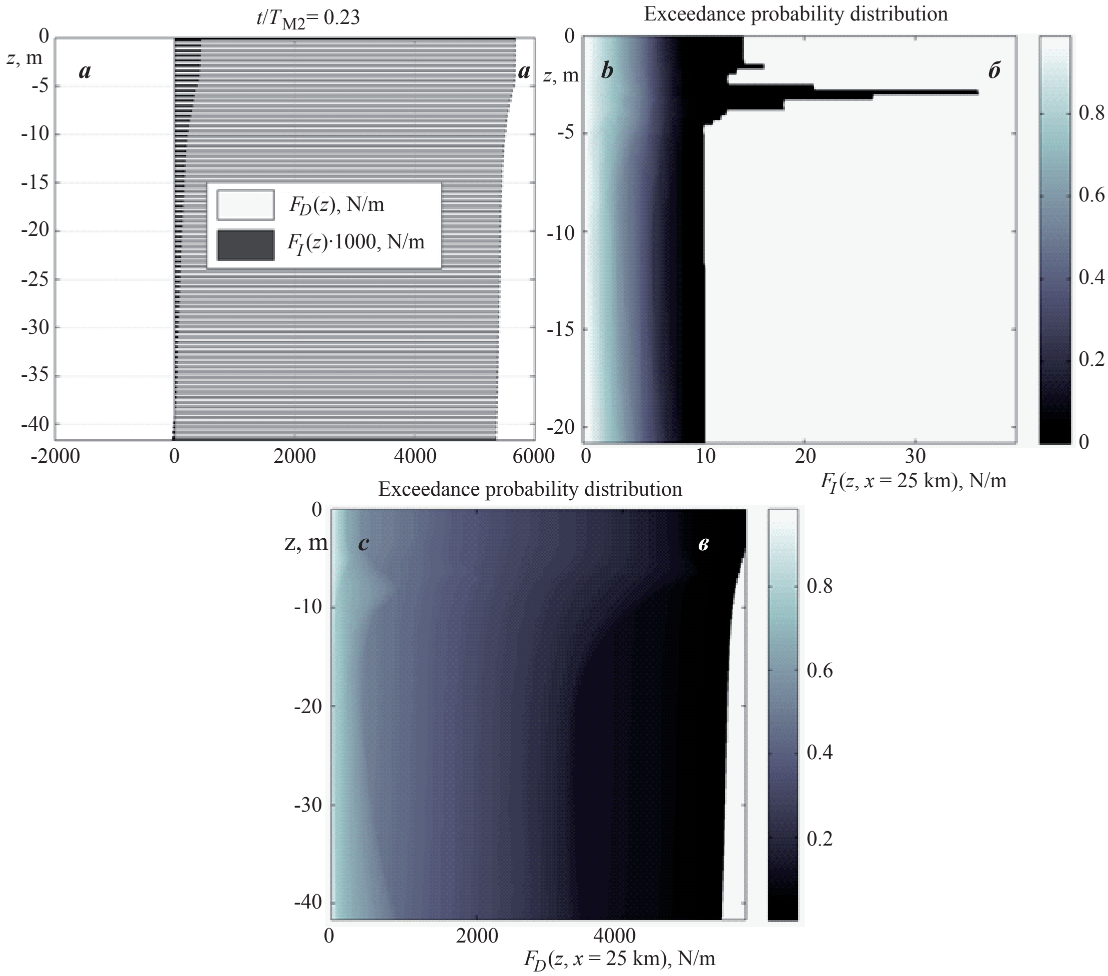

Fig. 7. The vertical distribution of the drag force and inertial force (both normalized for the unit length of the pile) intensity at the time of maximal impact (*a*); exceedance probability distributions of the inertial force (*b*) and drag force (*c*) intensity's absolute values (both normalized for the unit length of the pile).

Рис. 7. Вертикальное распределение интенсивности скоростной составляющей силы воздействия и инерционной компоненты (обе нормированы на единицу длины опоры) в момент максимального воздействия внутренних волн (*а*); распределение вероятности превышения уровня для абсолютных значений интенсивности инерционной силы (*б*) и скоростной составляющей волнового воздействия (*в*) (обе нормированы на единицу длины сваи).

To calculate shear forces and torques we determine the field of horizontal velocity (and acceleration) at the pile location (x = 25 km) over the total of the fluid column depending on time (fig. 5). As one can see, the velocity field becomes more irregular after some time due to the generation of internal waves.

Total shear force and the bending moment M′ (see eq. (3)) are shown in fig. 6. The characteristic length of internal waves is of order of hundreds of meters, so that the effect of pile with R = 2.5 m to the wave field can be ignored (i.e., $D/L < 0.15$). For the sake of simplicity, we choose the empirical coefficients $C_M = 1$ and $C_D = 1$ taking into account the considerations presented in [13] and fact, that both coefficients have an order of 1. The maximal absolute values of the force and the moment are reached at the first tidal cycle while there are no intensive internal waves and the structure of the current is still approximately barotropic. When internal waves are generating, the velocity/acceleration may have different signs at different depths. Let us consider a distribution of the loads upon unit length of the pillar at different times (fig. 7). In Morison equation, the force acting to a cylinder is a linear sum of a velocity-squared-dependent drag force and an acceleration-dependent inertial force. The inertial force is mainly smaller in absolute value than the drag force during this process (fig. 8). Graphs of exceedance probability distribution for both forces' intensities have visible spatial irregularity between $z = -5$ m and $z = -10$ m. This follows from the peculiarities of the vertical structure

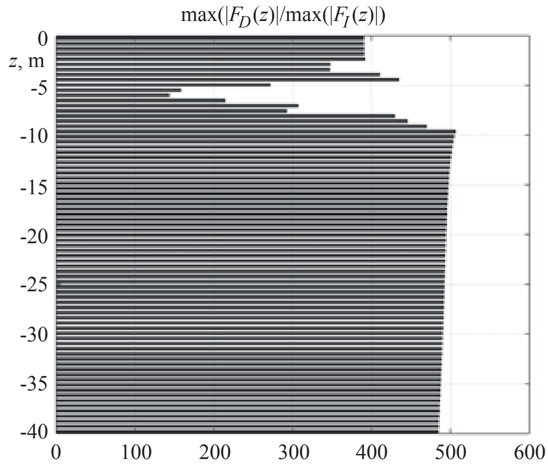

Fig. 8. The vertical distribution of the ratio of drag force maximal absolute value intensity to inertial force maximal absolute value intensity (both normalized for the unit length of the pile).

Рис. 8. Вертикальное распределение отношения максимального абсолютного значения интенсивности скоростной составляющей волнового воздействия к максимальному абсолютному значению интенсивности силы инерции (обе нормированы на единицу длины сваи).

of the horizontal velocity (see fig. 5) that show up due to generation of internal waves. At certain moments of time the inertial force can become comparable to drag force. Significant irregularity of the distribution of the load throughout the depth is the typical feature of the influence of internal waves.

***

The presented research focuses on possible scenarios of generation of internal waves from tidal wave in the shelf of Sakhalin Island area (Aniva Bay). Despite the relatively small depth spatial inhomogeneity of the selected section and the absence of generated solitons, the internal waves make their appreciable contribution to the investigated characteristics. We estimated the shear force and moment acting on a pile in such conditions on the basis of the calculated wave fields. It is estimated that intensity of lateral surface pressure and the rate inertia moment for a pile of 2.5 m diameter can reach values of $2.3 \cdot 10^5$ N and $4.8 \cdot 10^6$ N·m, respectively. Influence of internal waves manifests in significant irregularity of the distribution of the load in the vertical coordinate.

The results were obtained in the framework of the state task programme in the sphere of scientific activity of the Ministry of Education and Science of the Russian Federation (projects No. 5.4568.2017/6.7 and No. 5.1246.2017/4.6) and grants of the President of the Russian Federation (NSh-6637.2016.5 and SP-2311.2016.5).

References

1. *Bourgault D., Morsilli M., Richards C., Neumeier U., Kelley D.E.* Sediment resuspension and nepheloid layers induced by long internal solitary waves shoaling orthogonally on uniform slopes. *Continental Shelf Research.* 2014, 72, 21—33.
2. *Aghsaee P., Boegman L.* Experimental investigation of sediment resuspension beneath internal solitary waves of depression. *J. Geophys. Res. Oceans.* 2015, 120, 5, 3301—3314.
3. *Nishino S., Kawaguchi Y., Inoue J., Hirawake T., Fujiwara A., Futsuki R., Onodera J., Aoyama M.* Nutrient supply and biological response to wind-induced mixing, inertial motion, internal waves, and currents in the northern Chukchi sea. *J. Geophys. Res. Oceans.* 2015, 120, 3, 1975—1992.
4. *Wall M., Putchim L., Schmidt G. M., Jantzen C., Khokiattiwong S., Richter C.* Large-amplitude internal waves benefit corals during thermal stress. *Proceedings of the Royal Society of London B: Biological Sciences.* 2015, 282, 20140650.
5. *Wang Y.-H.* Phytoplankton transport to coral reefs by internal solitons in the northern south China sea. *Coral reefs.* 2016, 35, 3, 1061—1068.
6. *Rutenko A. N.* The influence of internal waves on losses during sound propagation on a shelf. *Acoustical Physics.* 2010, 56, 5, 703—713.
7. *Yang T. C.* Acoustic mode coupling induced by nonlinear internal waves: Evaluation of the mode coupling matrices and application. *Journal of the Acoustical Society of America.* 2014, 135, 2, 610—625.
8. *Wei G., Du H., Xu X., Zhang Y., Qu Z., Hu T., You Y.* Experimental investigation of the generation of large-amplitude internal solitary wave and its interaction with a submerged slender body. *Science China Physics, Mechanics and Astronomy.* 2014, 57, 2, 301—310.

9. *Cai S., Xu J., Chen Z., Xie J., Deng X., Lv H.* The effect of a seasonal stratification variation on the load exerted by internal solitary waves on a cylindrical pile. *Acta Oceanologica Sinica.* 2014, 33, 7, 21—26.
10. *Chakrabarti S.* Handbook of offshore engineering. *London, Elsevier*, 2005, 1321 p.
11. *Osborne A. R.* Nonlinear ocean waves and the Inverse Scattering Transform. *San Diego, Elsevier,* 2010, 944 p.
12. *Cai S., Long X., Gan Z.* A method to estimate the forces exerted by internal solitons on cylindrical piles. *Ocean Engineering.* 2003, 30, 5, 673—689.
13. *Cai S., Long X., Wang S.* Forces and torques exerted by internal solitons in shear flows on cylindrical piles. *Applied Ocean Research.* 2008, 30, 1, 72—77.
14. *Song Z. J., Teng B., Gou Y., Lu L., Shi Z. M., Xiao Y., Qu Y.* Comparisons of internal solitary wave and surface wave actions on marine structures and their responses. *Applied Ocean Research.* 2011, 33, 2, 120—129.
15. *Si Z., Zhang Y., Fan Z.* A numerical simulation of shear forces and torques exerted by large-amplitude internal solitary waves on a rigid pile in South China Sea. *Applied Ocean Research.* 2012, 37, 127—132.
16. *Xie J., Jian Y., Yang L.* Strongly nonlinear internal soliton load on a small vertical circular cylinder in two-layer fluids. *Applied Mathematical Modelling.* 2010, 34, 8, 2089—2101.
17. *Xie J., Xu J., Cai S.* A numerical study of the load on cylindrical piles exerted by internal solitary waves. *Journal of Fluids and Structures.* 2011, 27, 8, 1252—1261.
18. *Du T., Sun L., Zhang Y., Bao X., Fang X.* An estimation of internal soliton forces on a pile in the ocean. *J. Ocean Univ. China.* 2007, 6/2, 101—116.
19. *Newman J. N.* Marine Hydrodynamics. *Cambridge, MIT Press,* 1977, 402 p.
20. *Aleshkov Yu. Z.* The theory of the interaction of waves and obstacles. *Leningrad, LST Publ.,* 1990, 371 p. (in Russian).
21. *Khalfin I. Sh.* The impact of waves on the offshore oil and gas facilities. *Moscow, Nedra*, 1990, 312 p. (in Russian).
22. *Zhang D., Paterson E. G.* A study of wave forces on an offshore platform by direct CFD and Morison equation. *Proc. of 2nd Symposium on OpenFOAM in Wind Energy.* 2014, 1—34.
23. *Housseine C., Monroy C., de Hauteclocque G.* Stochastic Linearization of the Morison Equation Applied to an Offshore Wind Turbine. *Proc. ASME.* 56574; Volume 9: Ocean Renewable Energy, V009T09A040, May 31, 2015, OMAE2015-41301.
24. *Morison J. R., O'Brien M. P., Johnson J. W., Schaaf S. A.* The forces exerted by surface waves on piles. *Petroleum transactions, AIME.* 1950, 189, 149—157.
25. *Tovstik P. E., Tovstik T. M., Shekhovtsov A. S., Shekhovtsov V. A.* Motion of a flowing cylinder under waves. *Vestnik St. Petersburg Univ., ser. 1.* 2012, 3, 137—143 (in Russian).
26. *Lighhill M. J.* Fundamentals concerning wave loading on offshore structures. *Journal of Fluid Mechanics.* 1986, 173, 667—681.
27. *Tyugin D. Yu., Kurkin A. A., Pelinovsky E. N., Kurkina O. E.* Increase of productivity of software package for modeling of internal gravity waves IGW Research with the help of Intel® Parallel Studio XE 2013. *Fundamentalnaya i Prikladnaya Gidrofizika.* 2012, 5, 3, 89—95 (in Russian).
28. *Rouvinskaya E. A., Kurkina O. E., Kurkin A. A.* Modeling of internal weather in the ecosystem of the stratified sea shelf. *Ecological Systems and Devices.* 2011, 6, 8—16 (in Russian).
29. *Romanov A. A., Sedaeva O. S., Shevchenko G. V.* Seasonal and tidal variations of the sea level between Hokkaido and Sakhalin Islands based on satellite altimetry and coastal tide gauge data. *J. Pacific Oceanography.* 2004, 2, 117—125.